

SOFT SENSING WITH ECT IN PARTICULATE TRANSPORT WITH FOCUS ON BUBBLE CHARACTERIZATION

Ru Yan, Roshan Sharma, Håkon Viumdal, Saba Mylvaganam

University of South-Eastern Norway (www.usn.no), Department of Electrical Engineering, IT and Cybernetics, Faculty of Technology, Natural Sciences and Maritime Sciences, saba.mylvaganam@usn.no

Non-invasive sensors and soft-sensing using data fusion enable processes to be “seen” in real time. Electrical capacitance tomographic (ECT) system with an array of capacitance sensors on the periphery of a pipe transporting solid particles in fluidized bed columns (FBC) gives some vivid insight into bubble formation and behaviour of bubble swarms in the pipe. The tomographic/tomometric techniques give some valuable information on bubbles’ sizes, velocity and distributions in the FBCs. ECT data help to detect changes in distribution of particulates and by applying different data fusion algorithms involving autocorrelation, eigenvalues, probability density functions etc., and many parameters characterizing bubbles’ formation, transport and distribution are found, based on tests done in the FBCs. After describing the three-hopper silo system and its suite of sensors and the type of particulates used in the tests, the usage of the ECT system is described. Based on ECT sensors and data fusion, the following characteristics of particulate transport are found: radial variation of average solid fraction and average solid content over entire bed section, repeating patterns in bubble transport, identification of flow regimes and their transition regions and estimation of bubble sizes. Eigenvalues of the capacitance matrices obtained from the ECT system are also used in the characterization of bubbles. Support Vector Machine (SVM) is used for clustering of the raw data leads to identification of different particulate flow regimes. These methods in combination help in the identification of particulate flow regimes, bubble characterizations and hence in predicting flow regimes in FBCs.

KEY WORDS: fluidized bed, ECT, soft sensors, bubble characterisation, flow regimes.

1. FLUIDIZED BED COLUMN

Processes where solid particulates acquire properties of fluids, when these particulates are exposed to fluidizing agents such as pressurized air, occur in many industries. The pressurized air or gas depending on the aimed chemical reactions, is injected into the bed of particles with increasing flow velocity, which on reaching the fluidization velocity, produces bubbles in the bed of particles. Fluidization and these bubbles enhance the mass and heat transfer between the materials present in the bed and promotes intended chemical reactions. Many studies have been done on the formation of bubbles and the ensuing flow of particulate materials with the fluidizing air/gas, as in Dyakowski & Edwards (1997), Makkawi & Wright (2004), Sharma et al (2010) and Srivastava et al (1998). Referring Wang et al (1995), Zijerveld et al (1998), Datta et al (2007) and Yan et al (2012), the types

and sizes of particles, the fluidizing medium, its physical characteristics and flow rate lead to different flow regimes.

This paper collates results based on different techniques and gives a new perspective of data analytics in powder technology, with focus on FBCs. In this study, a fluidized bed column is used in studying fluidization of particles with focus on the flow regimes: fixed bed, fluidisation and slugging. During these three flow regimes, the fluidizing starting point and air inflow velocity for generating bubbling flow can be located. Based on these observations, control methods based on air inflow velocity can be developed. The vertical FBC used in this study with the mounted twin plane ECT-system is shown in Figure 1(a) with a corresponding schematic diagram showing the major modules in Figure 1(b).

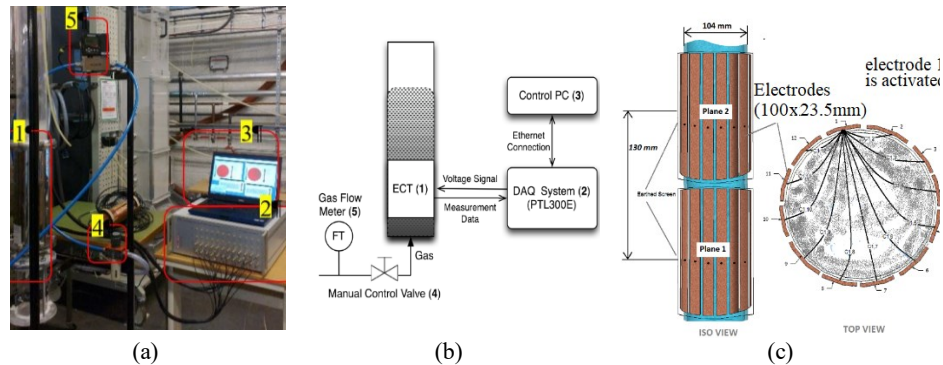


Figure 1. (a) Actual system used for fluidization studies using a fluidizing bed column (FBC) with a dedicated ECT measurement system; (b) Schematic diagram of the FBC with installed twin plane ECT sensor and its data acquisition and storage devices; (c) Geometry of the 12-electrodes twin-plane ECT sensor installed on the FBC as the item 1, and “TOP VIEW” shows as example the capacitance measurement between each pair of electrodes, with electrode no. 1 activated.

1.1 ELECTRICAL CAPACITANCE TOMOGRAPHY (ECT) SYSTEM

The ECT system with 12 electrodes is arranged in a single array as shown in Figure 1(c) in two planes with the characteristics given in Table 1. The system is positioned close to the bottom of the FBC to facilitate the monitoring of the material distribution in the sensing area through measuring the variations in the capacitance values between any pair of electrodes in the same sensor plane.

In this study, ECT image data are used to reconstruct 3D images that can provide useful information on flow regimes at different air inflow velocities. Capacitance volume ratios (CVR), computed direct from normalized capacitance values from ECT measurements are used in estimating bubble velocities and frequencies during ‘bubbling’ flow regime. Identification of flow regimes is also accomplished using the leading eigenvalues of the capacitance matrix obtained from the ECT-module.

1.2 EIGENVALUES FOR NORMALIZED CAPACITANCE MEASUREMENT

For an ECT-module with N -electrodes in one plane, a typical set of normalized capacitance measurements can be presented in a matrix form as:

$$CN(i, j, t) = \begin{cases} CN(i, j, t), & i < j \\ 0, & i \geq j \end{cases} \quad (1)$$

where CN is the normalized capacitance measurements; $i = 1 \dots, N$; $j = 1, 2, \dots, N$ and t represents time.

Equation (1) leads to a $N \times N$ upper triangular matrix with zeros on its diagonalelements, since typical ECT measurement systems skip the repetitions of the same inter-electrode combinations, because at any instant t , $C_{ij}(t) = C_{ji}(t)$, for the raw capacitances delivered by the ECT-module. Thus, for a set of measurements, usually called a “frame”, the complete capacitance matrix is given by:

$$CN(t)_{(u,v)} = \begin{cases} CN(i, j, t), & u \leq v; \quad i = u; \quad j = N + u - v \\ CN(j, i, t), & u > v; \quad i = N - u + v; \quad j = v \end{cases} \quad (2)$$

where, u and v are the index of row and column in the matrix respectively, $u = 1, \dots, (N-1)$; $v = 1, \dots, (N-1)$.

Eigenvalues of this new $(N-1) \times (N-1)$ matrix is calculated. The maximal eigenvalues in each vector is pointed out as the leading eigenvalue of each corresponding capacitance measurement frame. The seminal paper by Fang & Cumberbatch (2005) opened a new direction in ECT and reinforced the concept of electrical capacitance tomometric (ECTm). In the paper by Dupré et al (2016), the “crunching” of the eigenvalues is pursued further demonstrating the power of this technique in identifying the underlying flow regimes and material distribution leading to the ECT based raw capacitance measurements.

1.3 EXPERIMENTAL SETUP

The solid material used is glass particulates with density of 2485-2600kg/m³ with relative permittivity of approximately 4. Referring to Geldart’s powder classification pattern, it belongs to the class between type B, ‘sand like/bubbly’ when velocity is above minimal fluidization velocity, and type D, ‘spoutable’. Table 1 gives an overview of experimental setup information. Fluidizing fluid used through the test is air. The in flow air velocity increased gradually from 290 to 460 SLM (standard litre per minute) (corresponding to 0.569 to 0.903 m/s) within total 12 experiments.

Table 1

Main components and materials in the experimental setup shown in Figure 1

Modules/ materials in Figure 1	Characteristics/ Operating Conditions
Column pipe	Diameter = 104 mm, height = 1.5 m, material: cast acrylic
Distributor	Porous plate distributor
Fluidization medium	Air at ambient conditions (25 °C, 1 atm)
ECT system used	T win-plane with 12 electrodes/plane; 15 seconds data sampled at 100Hz
Air inflow velocity (SLM)	290, 312, 329, 340, 350, 365, 380, 395, 400, 411, 420, 460
Fluidized particulates	Spherical Ballotini glass particulates; average diameter of 850 μm -1000 μm; density 2600 kg/m ³

The airflow rate was gradually increased until fluidization occurred in the FBC. During each setting of airflow, raw capacitance data from the twin plane ECT for a time slot of 60s. The study of these data sets from the experiments with focus on bubble characteristics indicated that ECT data sampled at 100Hz and acquired in a time slot of 15 seconds, were enough to analyze the various calculations related to bubble characterizations

2. VISUALIZATION OF BUBBLE MOVEMENT

During bubble and slug flow, the bubble volume is always smaller than the sensing space, making it possible for the ECT to capture many 'redundant' measurements from bubble entering to existing the sensing area. This 'redundant' effect can be overcome, when reconstruction is done using the 3D flow image, by using only the pixels with positive variations during the "inflow" of bubbles into the sensing area; similarly, when bubbles are moving out from the sensing area, only the pixels with negative variations are used.

Figure 2 shows the reconstructed 3D images of the bubble movement under different air inflow conditions. From the reconstructed movements of bubbles presented in Figure 2, in the first three experiments (at airflows from 290 to 329 SLM) can be identified as 'bubbling' regime. However, already during the 3rd experiment, features indicating 'slugging' can be observed. From the 4th experiment (at an airflow of 340SLM), the flow has a transitional tendency from 'bubbling' to 'slugging'. When the airflow increased to 380SLM and to even higher speeds (from 8th to 12th experiment), the bubbles tend to occupy almost the entire cross section of the sensor plane. The flows corresponding to those observed during the 8th to 12th experiments belong to the 'turbulent' and 'fast fluidization' regimes.

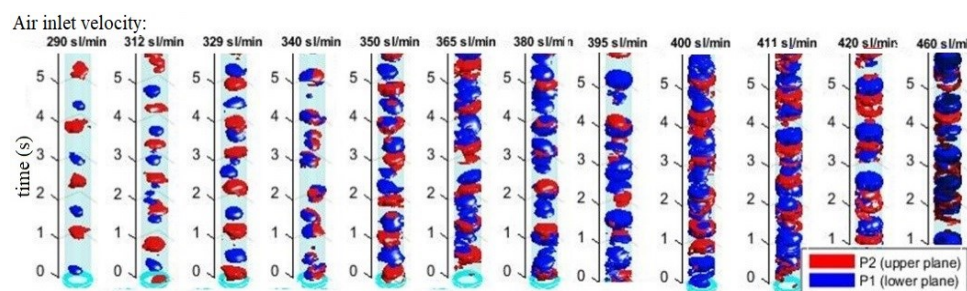


Figure 2. Reconstructed bubble images with airflow varying from 290 to 340SLM; 'blue' indicates the bubble generated from the lower ECT sensor plane (p1, relatively close to the bottom of bed and air inlet area); 'red' indicates the bubble generated from upper ECT sensor plane (p2).

3. BUBBLE CHARACTERIZATION ESTIMATION-VELOCITY AND FREQUENCY

Based on the results achieved in the last section, when airflow velocity is higher than 340SLM (after the 4th experiment), the flow appeared to be slugging and turbulent, during which bubbles' boundaries were not clear between the two sensor planes thus making it difficult or impossible to 'define' a complete bubble. Under these circumstances, it is

unrealistic to estimate neither bubble velocity nor bubble size, as an individual bubble was not discernable from the measurements or reconstructed images. Thus, the bubble velocity was estimated for the first four experiments only.

Figure 3(a) shows results from cross correlation of signals from the two planes of the ECT system, for the first experiment, showing 22 frames lag for the correlation peak, leading to an estimated bubble velocity of 0.3 m/s. All the estimated bubble velocities for the first four experiments are given in Figure 3(b). Referring to the estimated bubble frequency shown in Figure 4, we see a gradual increase in bubble frequency from the first to the fourth experiment. Figure 4 indicates that the bubble frequency at the lower sensor plane (P1) is higher than the bubble frequency at the upper plane (P2). These observations are reflected in the 3D images shown in Figure 2. From these results, it can be seen that the bubble velocity decreases from the 2nd to the 4th experiment, due to the bubble size increasing with increasing air inflow velocity.

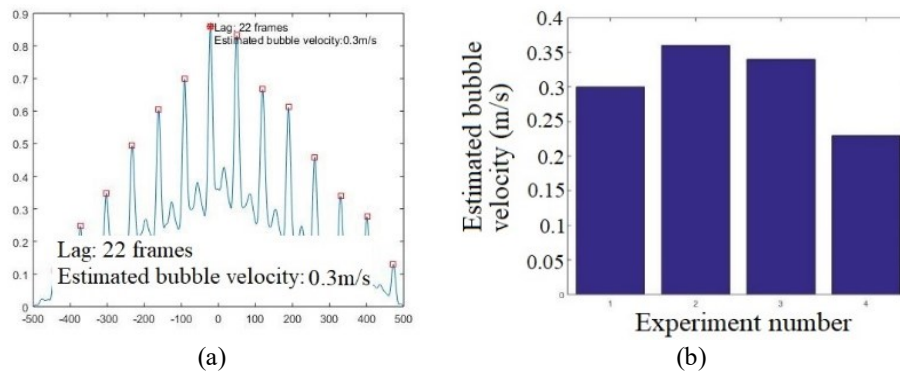


Figure 3. Cross-correlation based estimation of bubble velocity, 0.3 m/s, with air input flow rate at 292SLM; (b) estimated bubble frequency with the air inlet velocity from 290SLM to 340SLM

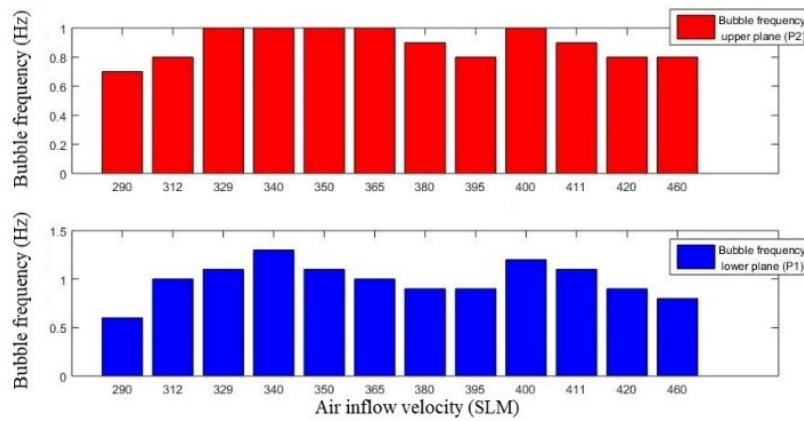


Figure 4. Estimated bubble frequency per second) in lower plane (blue) and in upper plane (red).

4. FLOW REGIME IDENTIFICATION DURING FLUIDIZATION

In the fluidizing process, the flow regime identification mostly depends on the variations in the characteristics of bubbles when the flow is moving upwards, i.e. especially on the variations of the particulate volume ratios between the two sensor planes. In this application, when using ECT sensor, both CVRs and leading eigenvalues show linear relationship with the volume ratios. Before using different data fusion techniques, we look into some pertinent data features, which is followed by some results based on leading algorithms and some established machine learning algorithms.

4.1 STUDY OF DATA FEATURES AND THEIR LINKS TO FLOW REGIMES

Figure 5(a) shows the variations of the RMS values of the ratio of the leading eigenvalues at planes P1 and P2. As can be seen in Figure 5(a), in the first 3 experiments, the RMS values do not increase much; from the 4th to 7th experiments, the RMS values increase significantly with increasing air inflow velocity; from 8th to 10th experiments the RMS values are more stable again until to the last two experiments.

Figure 5(b) shows the Gaussian Kernel Density Estimate (KDE) plot, which shows the distribution of 10 second averaged leading eigenvalues between the two sensor planes P1 and P2. The KDE curves from each experiment show clusters with the following pattern:

- Group 1: first two experiments are in this group;
- Group 1-2 (transition): from the 3rd experiment, the KDE curve starts to ‘connect’ to the next one;
- Group 2: from the 4th experiment, the KDE curve shows more “centres”;
- Group 3: from the 7th experiment, the KDE curves start to overlap each other;
- Group 4: from 11th to 12th experiment, isolated islands (cap) is formed with respect to the other KDE curves.

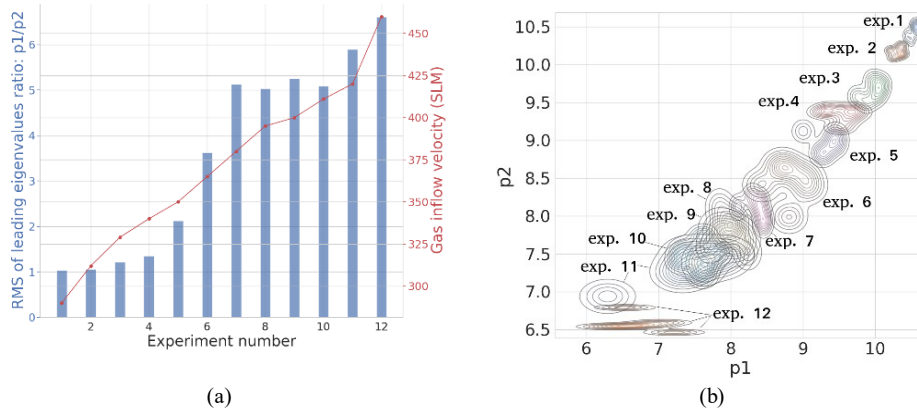


Figure 5. (a) RMS values of the ratios of leading eigenvalues for capacitance matrices measured at lower plane (P1) and upper plane (P2); the red dot and line plot is the corresponding air inflow velocity; (b) Kernel Density Estimate (KDE) plot: Data distribution of 10-second-averaged leading eigenvalues between P1 and P2

From these clusters by using KDE and leading eigenvalues, the raw capacitance values help to form the capacitance matrices for each frame, whose leading eigenvalues show characteristic patterns showing significant “fingerprint” behaviours, which can be associated with the different flow regimes. Fusion of these data features can enhance the identification process.

However, for a reliable control of the particulate flow behaviour in the FBC, the above observations are not sufficient for using them as inputs to the control system. Therefore, in the following sub-section 4.2, the classification results by using SVM are given.

4.2 STACKED SVM MODEL

Since there are mainly three types of flow regimes of interest in the context of this study, viz. ‘bubbling’, ‘slugging’ and ‘turbulent to pneumatic’ conveying, we need soft-sensing strategies to identified non-intrusively using the ECT system. In the results shown in this section, a stack-SVM (composed of two individual SVMs), radial basis function (RBF) kernel, is trained. In this stack of two blocks of SVM, two separate SVMs are used to classify 'bubbling / not bubbling' and 'slugging / turbulent and else' successively as illustrated in Figure 6.

For providing a ‘quick response’, the leading eigenvalues are averaged per second instead of 10 seconds (used in the case of KDE of Figure 5(b)). The inputs to stack-SVM are 1-second averaged leading eigenvalues from lower sensor plane (P1) and upper sensor plane (P2). Figure 6 shows the all averaged values for each experiment. In this plot, the dot size is dependent on the difference between the corresponding leading eigenvalues at the planes, P1 and P2.

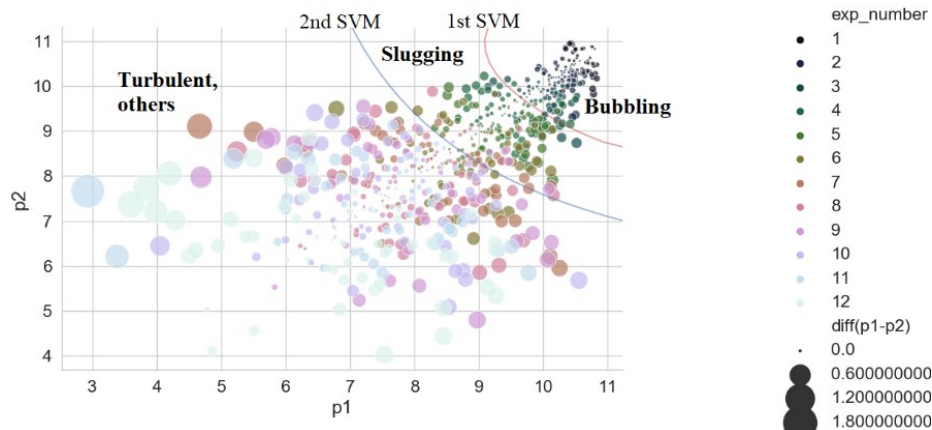


Figure 6. Overview of trained stacked SVM results; where 1st SVM (red hyperplane) is used to classify 'bubbling' and others; 2nd SVM (blue hyperplane) is used to classify between 'slugging' and 'turbulent, others'

The hyperplanes from the stack-SVM are also presented in the Figure 6. The first SVM gives an accuracy of 95.6%; and the second SVM gives an accuracy of 91.2%; the total stack-SVM gives an accuracy of 87%.

The first SVM (red hyperplane) is for recognition if the regime is ‘bubbling’ or not, performing at an accuracy of 95.6%; the second SVM (blue hyperplane) is for identifying the flow regime of ‘bubbling & slugging’ or ‘turbulent, others’, giving an accuracy of 91.2%.

The combination of the first SVM and the second SVM, gives for all these three flow regimes of interest an accuracy of identification of 87%. This is an acceptable result, especially as there are unclear transitions between the three flow regimes under scrutiny.

5. CONCLUSIONS

Using variations in ECT image pixel data, a stack of 3D images of bubbles is reconstructed using, time series from both sensor planes in a twin plane ECT-module. From these reconstructed 3D images, the difference between various flow regimes can be observed and identified with good accuracy. This is a method based on image processing. The bubble velocity and bubble frequency are estimated using the CVR data from both ECT sensor planes. From the results based on this method, we find that this method can be applied to identify bubble characteristics and bubble coalescence numerically.

Further, using a stack-SVM, the main fluidizing flow regimes can be identified through clustering the pattern from the averaged volume ratio from both sensor planes. The stack-SVM classification / identification results can deliver a unique output, such as a single number (index), e.g. ‘1’ for bubbling, ‘2’ for slugging, and so on. Therefore, the stacked SVM method has the potential for applications in real time control of processes involving FBC.

These results give useful information that can help to identify bubble velocity, frequency, location, coalescence and fluidization and flow regime identification. Thus, we suggest an automatic in-line real time control strategy of processes involving FBC based on these machine-learning methods as illustrated in Figure 7.

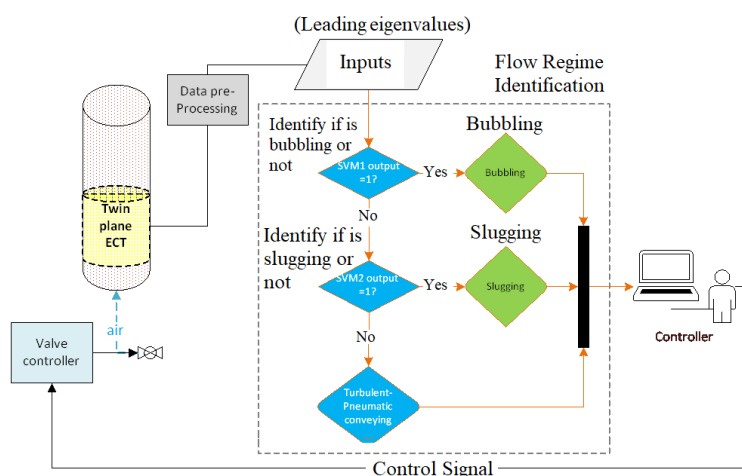


Figure 7. Flow chart of a FBC controller design scenario based on ECT sensor based on some machine-learning algorithms

REFERENCES

1. Datta, U, Dyakowski, T. and Mylvaganam, S., (2007), "Estimation of particulate velocity components in pneumatic transport using pixel based correlation with dual plane ECT", *Chemical Engineering Journal*, ISSN 1385-8947, e-ISSN 1873-3212
2. Dupré A., Ricciard, G., Bourennane S., Mylvaganam S. (2016) Identification of flow regimes using raw EIT measurements. 8th World Congress on Industrial Process Tomography, Brazil.
3. Dyakowski, T., Edwards, R. B., Xie, C. G., & Williams, R. A. (1997), "Application of capacitance tomography to gas–solid flows", *Chemical Engineering Science*, 52, 2099–2110.
4. Fang W. and Cumberbatch E. (2005) Matrix properties of data from electrical capacitance tomography, *Journal of Engineering Mathematics* vol.51, p. 127-146
5. Makkawi Y.T. and Wright P.C. (2004), "Electrical capacitance tomography for conventional fluidized bed measurements—remarks on the measuring technique", *Powder Technology* 148 142 –157.
6. Sharma, R., Karki, S., Masoudi, N., 2010, *Electrical Capacitance Tomography for characterizing bubble in fluidized beds*, Project Report, Telemark University College, Faculty of Technology.
7. Srivastava, A., Agrawal, K., Sundaresan, S., Karri, S. B., & Knowlton, T. M. (1998). Dynamics of gas-particle flow in circulating fluidized beds. *Powder Technology*, 100, 173–182.
8. Wange, S. J., Dyakowski, T., Xie, C. G., Williams, R. A., & Beck, M. S. (1995). Real time capacitance imaging of bubble formation at the distributor of a fluidized bed. *Chemical Engineering Journal*, 56, 11–16.
9. Yan, R.; Pradeep, C., Muwanga, J.; Mylvaganam, S. 'Interface Imaging in Multiphase Flow based on Frame by Frame Eigenvalues of Capacitance Matrices from Electrical Capacitance Tomographic Systems.' I: *Imaging Systems and Techniques (IST)*, 2012 IEEE International Conference on. IEEE conference proceedings 2012 ISBN 978-1-4577-1776-5. s. 466-469
10. Zijerveld, R. C., Johnsson, F., Marzocchella, A., Shoutten, J. C., & van den Bleek, C. M. (1998). Fluidization regimes and transition from fixed bed to dilute transport flow. *Powder Technology*, 95, 185–204.

